Research Article Vol. 42, No. 4 / April 2025 / Journal of the Optical Society of America A 495

Journal of the Optical Society of America A

OPTICS, IMAGE SCIENCE, AND VISION

Laguerre–Gaussian-to-Hermite–Gaussian mode conversion revisited

Somaye Fathollazade,[1] Saifollah Rasouli,[1,2,3,6] Davud Hebri,[4,*] Pouria Amiri,[1] and Sergey A. Ponomarenko[4,5]

[1]Department of Physics, Institute for Advanced Studies in Basic Sciences (IASBS), 444 Prof. Yousef Sobouti Blvd, Zanjan 45137-66731, Iran
[2]Center for International Scientific Studies and Collaboration (CISSC), Ministry of Science, Research and Technology, Tehran 15875-7788, Iran
[3]Optics Research Center, Institute for Advanced Studies in Basic Sciences (IASBS), Zanjan 45137-66731, Iran
[4]Department of Physics and Atmospheric Science, Dalhousie University, Halifax, Nova Scotia B3H 4R2, Canada
[5]Department of Electrical and Computer Engineering, Dalhousie University, Halifax, Nova Scotia B3J 2X4, Canada
[6]rasouli@iasbs.ac.ir
*d.hebri@dal.ca

Received 15 November 2024; revised 11 February 2025; accepted 23 February 2025; posted 25 February 2025; published 19 March 2025

We generalize a theoretical framework for Laguerre–Gaussian-to-Hermite–Gaussian (LG-to-HG) mode conversion induced by optical astigmatism and identify threea distinct conversion scenarios depending on the astigmatism conditions. We analyze the LG beam diffraction by three types of astigmatic optical elements, cylindrical lenses, quadratic curved-line gratings, and off-axis illuminated elliptical zone plates, and show that the LG modes of different orders convert to the corresponding HG modes over different distances, if at all. We explore two families of astigmatic phase profiles that offer independent control over the stretching and orientation of the converted modes. Our theoretical predictions are in good qualitative agreement with experimental results. © 2025 Optica Publishing Group. All rights, including for text and data mining (TDM), Artificial Intelligence (AI) training, and similar technologies, are reserved.

https://doi.org/10.1364/JOSAA.547816

1. INTRODUCTION

Laguerre–Gaussian (LG) beams, with their signature annular transverse intensity profile, have attracted substantial interest since Allen *et al.* introduced the concept of orbital angular momentum (OAM) associated with these beams [1,2]. The LG beams possess azimuthal (l) and radial (p) quantum numbers (indices), endowing them with additional degrees of freedom. Vortex beams, including the LG beams, exhibit reduced distortion when traversing optical turbulence compared to Gaussian beams [3]. Consequently, such beams have diverse applications across various fields [4,5], including optical manipulation [6], microfluidics [7], free-space communications [8], and quantum information processing [9]. Notably, LG beams with nonzero radial indices can trap multiple particles along concentric circular paths, inducing orbital rotation due to the presence of multiple intensity rings around the beam axis. This versatility makes them valuable for advanced optical applications. Numerous techniques have been developed for generating and characterizing optical vortices. The pioneering experimental work on the generation of OAM waves was performed by Allen *et al.* in 1992 [10]. They employed cylindrical lenses arranged in a specific configuration in front of Hermite–Gaussian (HG) modes to produce various LG modes. Additional methods include interference techniques [11], diffraction from apertures [12–15], and the application of robust mode converters [16]. Additionally, cylindrical lenses have been employed for the characterization of LG beams with zero and nonzero radial indices [17–19], and a method based on analyzing diffraction patterns through a tilted biconvex lens has been introduced in Ref. [20] as well. Previous studies also explored the diffraction of optical vortex beams from gratings [21–25] and examined the Talbot effect with vortex beams [26]. Recently, we have carried out extensive research on LG beams using quadratic curved-line gratings. Specifically, we characterized single optical vortex with zero and nonzero radial indices [27,28], as well as collinear and on-axis combinations of two optical vortices with different winding numbers [29]. Furthermore, our recent study investigated the diffraction of vortex beams with nonzero quantum numbers from a binary grating characterized by a small opening ratio. This work paved the way for an alternative method for transforming LG beams into HG ones [30].

The HG and LG beams are subsets of a broader family known as Hermite–Laguerre–Gauss (HLG) beams, $\mathcal{G}_{m,n}(\mathbf{r}|\alpha)$. The HLG beams were initially introduced in Ref. [31] as the astigmatically transformed HG beams. The main properties of these beam families have been presented in Ref. [32]. The general astigmatic transform of HLG beams has been discussed in Ref. [33].

In this work, we refine the theoretical framework for LG-to-HG mode conversion via astigmatism and introduce an alternative approach based on expanding LG modes in terms of HG modes. Our analysis reveals three distinct mode conversion behaviors depending on the astigmatism conditions: conversion occurring at a specific propagation distance, conversion occurring at two separate distances, or no conversion at all. To systematically characterize these behaviors, we present two-dimensional color-coded maps in the astigmatism parameter space, where each color represents one of the three possible conversion cases. We apply this framework to analyze the LG beam diffraction by three types of astigmatic optical elements: cylindrical lenses, quadratic curved-line gratings, and off-axis illuminated elliptical zone plates (ZPs). We demonstrate that LG-to-HG mode conversion is diffraction-order dependent for the latter two elements, leading to distinct conversion distances for different orders. Additionally, we investigate the far-field propagation of astigmatic LG beams using two independent analytical methods, yielding a Fourier-based formulation involving Hermite polynomials. This result has potential applications beyond paraxial optics. Finally, we explore two families of astigmatic phase profiles that enable controlled LG-to-HG mode conversion, providing independent control over the stretching and orientation of the converted modes. Our findings provide a deeper understanding of LG beam interactions with astigmatic optical elements, paving the way for their optimized use in optical communications, microparticle manipulation, and structured beam microscopy. The insights gained from this study contribute to the broader field of structured light, offering new avenues for beam shaping, mode conversion, and advanced optical applications.

2. HERMITE–GAUSSIAN, LAGUERRE–GAUSSIAN, AND HERMITE–LAGUERRE–GAUSSIAN BEAMS

This section provides a concise review of three well-known beam families, namely HG, LG, and HLG beams. The paraxial evolution of a coherent light field in the coordinates $(\mathbf{r}, z) = (x, y, z) = (r\cos\theta, r\sin\theta, z)$ propagating in free space along the z axis is governed by the well-known paraxial Helmholtz equation [34]

$$\left(\partial_x^2 + \partial_y^2 + 2ik\partial_z\right)\Psi = 0, \tag{1}$$

where $k = 2\pi/\lambda$ denotes the wavenumber. Given the complex amplitude of a light field in the $z = 0$ plane, $\Psi(\mathbf{r}, 0)$, its propagation is described by the Fresnel transform

$$\Psi(\mathbf{r}, z) = \mathrm{FR}_z\left[\Psi(\mathbf{r}, 0)\right] = \frac{1}{i\lambda z}\iint_{\mathbb{R}^2} e^{i\gamma|\mathbf{r}-\mathbf{r}'|^2}\Psi(\mathbf{r}', 0)\mathrm{d}\mathbf{r}', \tag{2}$$

where $\gamma = \pi/(\lambda z)$ is a real parameter inversely proportional to z and λ. Before proceeding, we consider the following interesting attribute of the Fresnel transform [30]:

$$\mathrm{FR}_z\left[\sum_{q=-\infty}^{+\infty} t_q e^{i\frac{2\pi q x}{\Lambda}} u_q(x, y, 0)\right]$$

$$= e^{i\gamma x^2}\sum_{q=-\infty}^{+\infty} t_q e^{-i\gamma x_q^2} u_q(x_q, y, z), \tag{3}$$

where $x_q = x - \frac{q\lambda z}{\Lambda}$ and $u_q(\mathbf{r}, z) = \mathrm{FR}_z[u_q(\mathbf{r}, 0)]$.

Two well-known solutions of the paraxial equation are the HG and LG functions [35]

$$\mathcal{H}_{m,n}(\mathbf{r}) = e^{-(x^2+y^2)} H_m\left(\sqrt{2}x\right) H_n\left(\sqrt{2}y\right), \tag{4a}$$

$$\mathcal{L}_p^l(\mathbf{r}) = e^{-(x^2+y^2)}(x \pm iy)^{|l|} L_p^{|l|}\left[2\left(x^2+y^2\right)\right], \tag{4b}$$

where l and p are the topological charge (TC) and radial index of an LG mode, and sign $+$ or $-$ corresponds to the case $l > 0$ or $l < 0$, respectively. These two beam families are subsets of a broader family known as HLG beams, $\mathcal{G}_{m,n}(\mathbf{r}|\alpha)$, expressed as [32,36]

$$\mathcal{G}_{m,n}(\mathbf{r}|\alpha) = \sum_{k=0}^{m+n} i^k c_k^{(m,n)}(\alpha)\mathcal{H}_{m+n-k,k}(\mathbf{r}). \tag{5}$$

Here $c_k^{(m,n)}(\alpha) = \cos^{m-k}(\alpha)\sin^{n-k}(\alpha) P_k^{(m-k,n-k)}(-\cos 2\alpha)$, where $\alpha \in \mathbb{R}$, and $P_k^{(\mu,\nu)}(x)$ indicates Jacobi polynomials. In the special cases $\alpha = 0$ and $\alpha = \pi/4$, we have [33]

$$\mathcal{G}_{m,n}(\mathbf{r}|0) = (-i)^n \mathcal{H}_{m,n}(\mathbf{r}), \tag{6a}$$

$$\mathcal{G}_{m,n}(\mathbf{r}|\pi/4) = (-1)^{\min} 2^{\max} \min!\mathcal{L}_{\min}^{m-n}(\mathbf{r}), \tag{6b}$$

where $\min = \min(m, n)$ and $\max = \max(m, n)$. We can rewrite Eq. (6b) as

$$\mathcal{L}_p^l(\mathbf{r}) = \frac{(-1)^p}{p!2^{p+|l|}}\begin{cases}\mathcal{G}_{p+|l|,p}(\mathbf{r}|\pi/4), & l \geq 0;\\ \mathcal{G}_{p,p+|l|}(\mathbf{r}|\pi/4), & l < 0.\end{cases} \tag{7}$$

3. PROPAGATION OF AN LG BEAM WITH ASTIGMATISM: GENERAL THEORETICAL FORMULATION

Let us now review the propagation of an LG beam possessing astigmatism, as examined in Refs. [33,37], using a slightly different notation. The field profile just in front of an astigmatic element is an ideal LG beam, namely $\Psi(\mathbf{r}, -0) = \mathcal{L}_p^l(\mathbf{r}/w_0)$, where w_0 is the spot size at $z = 0$. Astigmatism is imparted to the field at the source plane, $z = 0$, and is defined by the curvature difference between the x and y directions [33,37]:

$$\Psi(\mathbf{r}, +0) = \exp\left[i\left(c_x\frac{x^2}{w_0^2} + c_y\frac{y^2}{w_0^2}\right)\right]\mathcal{L}_p^l(\mathbf{r}/w_0), \tag{8}$$

where c_x and c_y are dimensionless real parameters. In Supplement 1, we show that astigmatic elements do not affect the OAM of the beam. By introducing the auxiliary parameters

$$\zeta = \frac{z}{z_R}, \quad \sigma_x = 1 + c_x\zeta + i\zeta, \quad \sigma_y = 1 + c_y\zeta + i\zeta,$$

$$\omega_\pm = \frac{\arg\sigma_y \pm \arg\sigma_x}{2}, \tag{9}$$

where $z_R = \pi w_0^2/\lambda$ is a Rayleigh range, the beam evolution is governed by a Fresnel transform, resulting in [33] as follows:

$$\Psi(\mathbf{r},z)\propto\frac{e^{i[\Phi(\mathbf{r})+\Theta]}}{\sqrt{|\sigma_x\sigma_y|}}\begin{cases}\mathcal{G}_{p+|l|,p}\left[\mathrm{R}\left(-\frac{\pi}{4}\right)\mathbf{r}_1|\frac{\pi}{4}-\omega_-\right], & l\geq 0;\\ \mathcal{G}_{p,p+|l|}\left[\mathrm{R}\left(-\frac{\pi}{4}\right)\mathbf{r}_1|\frac{\pi}{4}-\omega_-\right], & l<0.\end{cases} \tag{10}$$

Here

$$\mathrm{R}(\vartheta)=\begin{pmatrix}\cos\vartheta & -\sin\vartheta\\ \sin\vartheta & \cos\vartheta,\end{pmatrix} \tag{11}$$

is the rotation matrix by an angle ϑ in the transverse plane of the beam and

$$\mathbf{r}_1=\left(\frac{x}{w_0|\sigma_x|},\frac{y}{w_0|\sigma_y|}\right), \tag{12a}$$

$$\Phi(\mathbf{r})=\frac{c_x+(1+c_x^2)\zeta}{w_0^2|\sigma_x|^2}x^2+\frac{c_y+(1+c_y^2)\zeta}{w_0^2|\sigma_y|^2}y^2, \tag{12b}$$

$$\Theta=l(\pi/4)-(2p+|l|+1)\omega_+. \tag{12c}$$

For some values of c_x, c_y, and ζ for which $\omega_-=\pi/4$, an LG-to-HG mode conversion takes place. Using the relation

$$\arctan(a)-\arctan(b)=\arctan\left(\frac{a-b}{1+ab}\right), \tag{13}$$

and considering $\lim_{\vartheta\to 0}\tan(\vartheta)=\pm\infty$, the condition $\omega_-=\pi/4$ leads to a quadratic equation in terms of ζ as [33]

$$(1+c_xc_y)\zeta^2+(c_x+c_y)\zeta+1=0. \tag{14}$$

This quadratic equation identifies the propagation distances at which the conversion of LG to HG modes occurs. These propagation distances can be obtained by

$$\zeta=\frac{-(c_x+c_y)\pm\sqrt{(c_x-c_y)^2-4}}{2(1+c_xc_y)}. \tag{15}$$

Equation (15) yields acceptable values for ζ only if they are real and positive. Then acceptable values of ζ require $|c_x-c_y|\geq 2$. To examine the roots of Eq. (14), we can express it as $\zeta^2-S\zeta+P=0$, where S and P represent the sum and product of the roots, respectively. Consequently, we get

$$S=-\frac{c_x+c_y}{1+c_xc_y},\qquad P=\frac{1}{1+c_xc_y}. \tag{16}$$

When $|c_x-c_y|=2$, Eq. (14) has a single, repeated root. Positive roots require both $P>0$ and $S>0$, leading to the conditions $c_xc_y>-1$ and $(c_x+c_y)<0$. When $|c_x-c_y|>2$, Eq. (14) has two distinct roots. This presents three possibilities: both roots are positive, both roots are negative, or they have opposite signs. The first possibility requires $c_xc_y>-1$ and $(c_x+c_y)<0$, the second one requires $c_xc_y>-1$ and $(c_x+c_y)>0$, while the latter requires $c_xc_y<-1$. Then LG-to-HG mode conversion during the propagation occurs zero, one, or two times depending on the values of c_x and c_y. Two conversions occur when $|c_x-c_y|>2$, $c_xc_y>-1$, and $(c_x+c_y)<0$. A single conversion occurs when either $|c_x-c_y|>2$, $c_xc_y<-1$, or when $|c_x-c_y|=2$, $c_xc_y>-1$, and $(c_x+c_y)<0$. Otherwise, no LG-to-HG mode conversion occurs. Figure 1 shows the values of c_x and c_y for which LG-to-HG mode conversion occurs once, twice, or never. Figure 2 shows the propagation of an LG beam with $p=1$ and $l=3$ possessing astigmatism, based on Eq. (8), having various values of c_x and c_y. The LG-to-HG mode conversion occurs once, twice, or never during the propagation depending on the values of c_x and c_y. The values of (c_x, c_y) used in the first to sixth rows of Fig. 2 are shown with the letters A–F in Fig. 1.

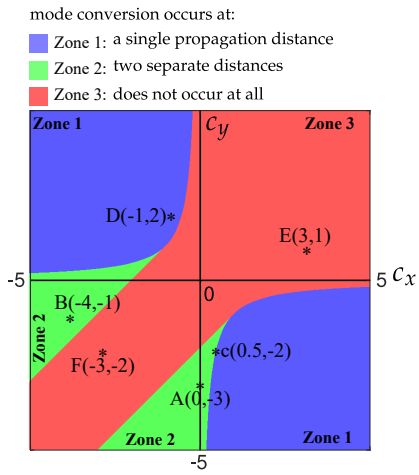

Fig. 1. Values of c_x and c_y for which LG-to-HG mode conversion occurs once (Zone 1), twice (Zone 2), or never (Zone 3).

Moreover, considering the special case $c_xc_y=-1$, which corresponds to the boundary of the blue region in Fig. 1, Eq. (14) reduces to a linear equation whose root is

$$\zeta=\frac{1}{c_x^{-1}-c_x}. \tag{17}$$

This is an acceptable answer provided that $0<c_x<1$ or $c_x<-1$. As an example, the case $c_x=0.5$ and $c_y=-2$ is illustrated in the third row of Fig. 2, where LG-to-HG mode conversion occurs once at the propagation distance predicted by Eq. (17). The background Visualization 1 illustrates the evolution of an astigmatic LG beam with $l=3$ and $p=1$ for variables c_x and c_y.

As an alternative approach, we can expand an LG mode into HG modes and obtain, after straightforward calculations spelled out in Supplement 1, we obtain

$$\begin{aligned}\Psi(\mathbf{r},z)\propto{}&\gamma w_xw_y e^{i\gamma r^2}e^{-\gamma^2\left(w_x^2x^2+w_y^2y^2\right)}\\ &\times\sum_{n=0}^{p}\sum_{m=0}^{|l|}c_{m,n}^{\pm}e^{i(n_1\phi_x+n_2\phi_y)}H_{n_1}\left(\frac{\sqrt{2}\gamma|w_x|^2x}{w_0}\right)\\ &\times H_{n_2}\left(\frac{\sqrt{2}\gamma|w_y|^2y}{w_0}\right).\end{aligned} \tag{18}$$

Here $c_{m,n}^{\pm}$ is defined in Eq. (S5) of Supplement 1, $n_1=|l|+2n-m$, and $n_2=2p-2n+m$. Furthermore,

$$w_x=\frac{w_0}{\sqrt{1-i(c_x+z_R/z)}},\qquad w_y=\frac{w_0}{\sqrt{1-i(c_y+z_R/z)}}, \tag{19a}$$

$$\phi_x=\arctan\left(c_x+\frac{z_R}{z}\right),\qquad \phi_y=\arctan\left(c_y+\frac{z_R}{z}\right). \tag{19b}$$

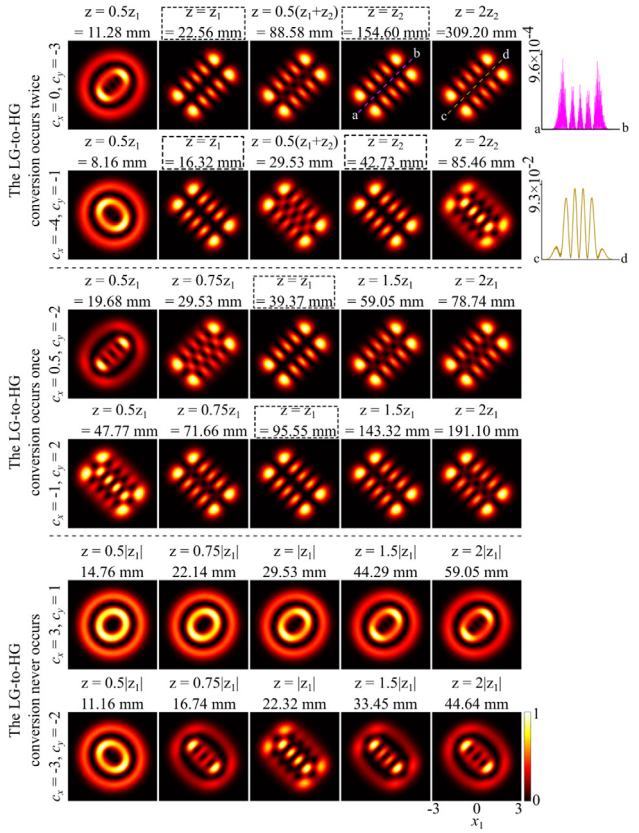

Fig. 2. Propagation of an LG beam with $p = 1$ and $l = 3$ influenced by astigmatism having various values of c_x and c_y so that LG-to-HG mode conversion occurs once (first and second rows), twice (third and fourth rows), or never (fifth and sixth rows). All patterns are depicted in stretched coordinates (x_1, y_1) defined by Eq. (12a). For additional details, see also Visualization 1.

Equation (18) offers several advantages over Eq. (10). The key advantage is the latter involves both Hermite and Jacobi polynomials, while the former is expressed solely in terms of Hermite polynomials and does not involve a removable singularity at $\omega_- = \pi/4$. This circumstance makes our representation especially suitable for numerical simulations.

Next, specifying to the case $p = 0$, after some algebra outlined in Supplement 1, we can simplify Eq. (18) as

$$\Psi(\mathbf{r}, z) \propto \gamma w_x w_y e^{i\gamma r^2} e^{-\gamma^2\left(w_x^2 x^2 + w_y^2 y^2\right)} \varphi^{|l|}(z) H_{|l|} \times \left[\frac{\sqrt{2}\gamma\left(|w_x|^2 e^{i\phi_x} x \pm i|w_y|^2 e^{i\phi_y} y\right)}{w_0 \varphi(z)}\right], \quad (20)$$

where $\varphi(z) = \sqrt{e^{2i\phi_x} - e^{2i\phi_y}}$. This is similar to the equation obtained in Ref. [18] for the case where $p = 0$.

4. CONVERGING CYLINDRICAL LENS AS AN OPTICAL ELEMENT WITH ASTIGMATIC PHASE ABERRATION

We can write the transmittance function of a converging cylindrical lens as [38]

$$t(x) = \exp\left(-\frac{i\pi x^2}{\lambda f}\right), \quad (21)$$

where f is the focal length of the lens. By comparing Eq. (21) with the general astigmatism form in Eq. (8), we find $c_x = -z_R/f$ and $c_y = 0$. Therefore, the diffraction of an LG beam from a converging cylindrical lens can be predicted employing Eq. (10) or Eq. (18) only setting $c_x = -z_R/f$ and $c_y = 0$. Furthermore, substituting these values into Eq. (14) determines the propagation distances for LG-to-HG mode conversion. By substituting $c_x = -z_R/f$ and $c_y = 0$ in Eq. (15), we get

$$\zeta = \frac{z_R}{2f}\left[1 \pm \sqrt{1 - \left(\frac{2f}{z_R}\right)^2}\right]. \quad (22)$$

Obviously, the LG-to-HG mode conversion requires $2f \le z_R$ or equivalently $w_0 \ge \sqrt{2f\lambda/\pi}$. As we typically have $f \ll z_R$, the following estimation is reasonable:

$$\zeta_1^{\text{app}} \approx \frac{f}{z_R}, \quad \zeta_2^{\text{app}} \approx \frac{z_R}{f}, \quad (23)$$

where we used $\sqrt{1-x^2} \approx 1 - \frac{1}{2}x^2$ for $x \ll 1$. Then the propagation distances can be estimated as follows:

$$z_1^{\text{app}} \approx f, \quad z_2^{\text{app}} \approx z_R^2/f. \quad (24)$$

In Fig. 3, we display—see left to right—an LG beam with $p = 2$ and $l = \pm 2$, a converging cylindrical lens with a focal length $f = 16.5$ cm and the corresponding diffraction pattern in the focal plane of the lens. The insets show horizontally enlarged images of the diffraction patterns. As expected, LG-to-HG mode conversion takes place in the focal plane of the cylindrical lens. The intensity pattern appears tightly focused due to the action of the cylindrical lens. However, this pattern can be stretched to better reveal the LG-to-HG mode conversion. The resulting intensity distribution forms a two-dimensional array of spots, which depends on the beam's TC

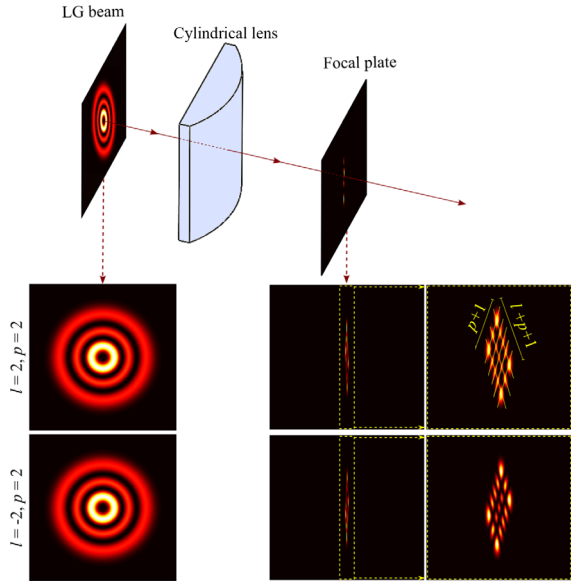

Fig. 3. Empirical arrangement illustrating the diffraction of (LG) beams with $p = 2$ and azimuthal index $l = \pm 2$ using a cylindrical lens.

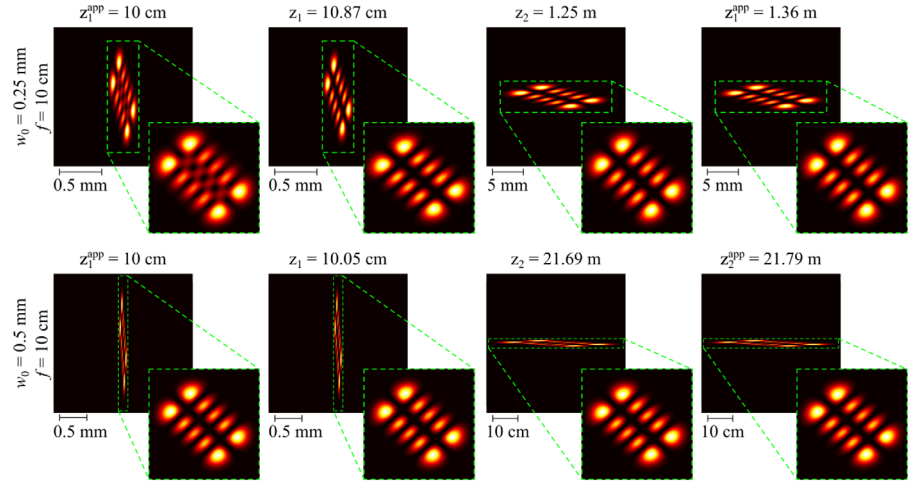

Fig. 4. Diffraction patterns of LG beams having $\lambda = 532$ nm, $p = 1$, $l = 3$, $w_0 = 0.25$ mm (first row), and $w_0 = 0.5$ mm (second row) from a cylindrical lens with $f = 10$ cm at exact and estimated distances, respectively, obtained from Eqs. (22) and (24). All insets are depicted in stretched coordinates (x_1, y_1) defined by Eq. (12a).

and radial index. By counting these spots, the TC and radial index can be determined.

To validate Eqs. (22) and (24), in Fig. 4, we depict the diffraction of LG beams with $\lambda = 532$ nm, $w_0 = 0.25$ mm (first row), and $w_0 = 0.5$ mm (second row) from a cylindrical lens with $f = 10$ cm at exact and estimated distances. Obliviously, the LG-to-HG mode conversion occurs at exact distances. The Rayleigh ranges are $z_R \approx 37$ cm (first row) and $z_R \approx 1.5$ m (second row). Consequently, the condition $f \ll z_R$ is satisfied only in the second row, resulting in LG-to-HG mode conversion at both the exact and estimated distances.

The experimental setups used in this study are illustrated in Fig. 5. The beam generation section features an Nd:YAG diode-pumped laser operating at a wavelength of $\lambda = 532$ nm. A beam expander system, comprising a spatial filter and a collimating lens, ensures proper beam collimation. The collimated beam then interacts with multicircle phase-shifted amplitude fork gratings exhibiting a sinusoidal profile, characterized by central and intermediate radial phase discontinuities [39]. The radial index and TC of the generated LG beam depend on the fork's charge and the number of surrounding phase discontinuity rings.

In the LG beam generation section, a specific diffraction order of the output LG beams from the amplitude gratings is selected, while the remaining orders are blocked. The selected beam then encounters an astigmatic optical element. For diffraction-based elements, an additional obstacle is employed to eliminate unwanted diffraction orders, as shown in Fig. 5(b).

The characterization section, also referred to as the LG-to-HG conversion section, follows a similar approach: one diffraction order of the output LG beams is isolated, while the others are suppressed. Figure 5(a) illustrates the optical characterization setup with a cylindrical lens, where the two-way arrow indicates the positions at which images are captured by a Nikon D7200 camera, both before and after the focal plane. Figure 5(b) depicts an alternative setup utilizing either a curved linear amplitude grating or an off-axis elliptical ZP loaded onto a spatial light modulator (SLM) (3M X50, resolution:

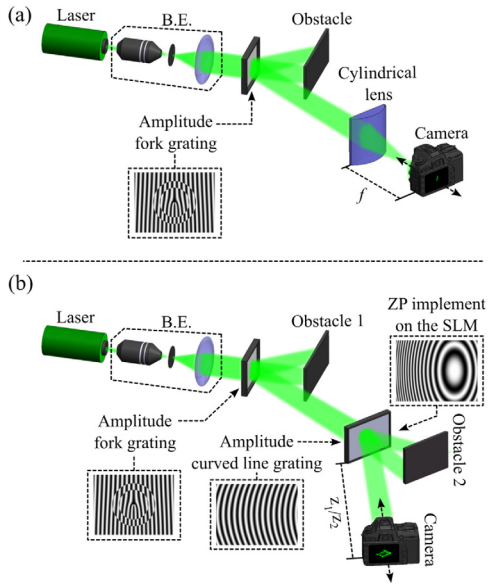

Fig. 5. Experimental setups used in this study. (a) Optical characterization setup employing a cylindrical lens, where the two-way arrow indicates the positions at which images are captured by a Nikon D7200 camera, both before and after the focal plane. (b) Alternative setup featuring either a curved linear amplitude grating or an off-axis elliptical zone plate (ZP) loaded onto a spatial light modulator (SLM). In the case of an off-axis elliptical grating, the displacement is adjusted to shift the ellipse's center horizontally or vertically.

1024 × 768, display: 0.7 in. polysilicon LCD). When an off-axis elliptical ZP is used, the displacement is adjusted so that the center of the ellipse is shifted from the origin either horizontally or vertically.

In Fig. 6, we exhibit experimental (bottom row) and theoretical (top row) results obtained from Eqs. (10) and (18) for an LG beam with $l = 2$, $p = 2$, and $w_0 = 0.8$ mm transmitted through a cylindrical lens with $f = 16.5$ cm at a variable propagation distance in the vicinity of the focal plane of the lens. The figure clearly confirms good qualitative agreement between the theory

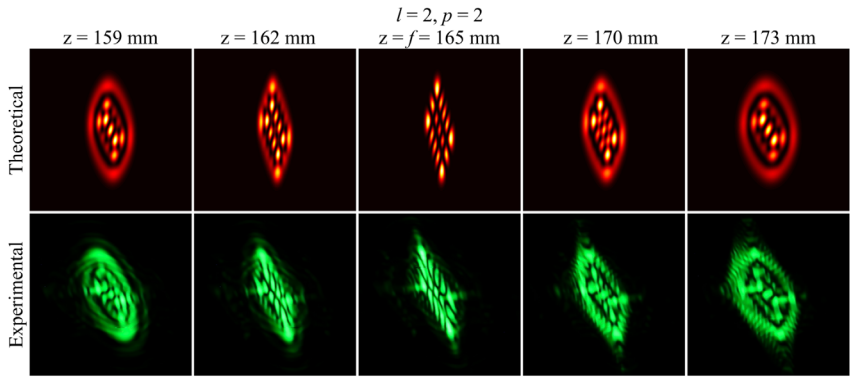

Fig. 6. Theoretical (top row) and experimental (bottom row) results of the diffraction of an LG beam with $l = 2$, $p = 2$, and $w_0 = 0.8$ mm from a cylindrical lens with $f = 16.5$ cm in different propagation distances before and after focal length. For additional details, see also Visualization 2.

and experiment, thereby testifying to the validity of our theoretical framework. In background Visualization 2, a calculated diffraction pattern of an LG beam from a cylindrical lens under propagation is presented, effectively demonstrating the effect of astigmatism aberration on the LG beam.

5. QUADRATIC CURVED-LINE GRATING AS AN ASTIGMATIC OPTICAL ELEMENT

We can consider a quadratic curved-line structure (parabolic line) periodic along the x axis similar to a conventional grating. In contrast, its functionality along the y axis is similar to a 1D zone plate [27–29]. Therefore, the characteristic parameters of a quadratic curved-line structure are the period Λ and the focal length f for an incident beam with a wavelength λ, and its transmission function is an arbitrary periodic function with a period of Λ, which can be expressed as a Fourier series as

$$t(\mathbf{r}) = \sum_{q=-\infty}^{+\infty} t_q \exp\left[i2\pi q\left(\frac{x}{\Lambda} - \frac{y^2}{2\lambda f}\right)\right]. \tag{25}$$

Let us now consider the diffraction of an LG beam from a quadratic curved-line grating. The complex amplitude immediately after the grating can be expressed as

$$\Psi(\mathbf{r}, +0) = \mathcal{L}_p^l(\mathbf{r}/w_0)t(\mathbf{r}). \tag{26}$$

Equation (26) can be rewritten as

$$\Psi(\mathbf{r}, +0) = \sum_{q=-\infty}^{+\infty} t_q \exp\left(i\frac{2\pi qx}{\Lambda}\right) u_q(\mathbf{r}, 0), \tag{27}$$

where $u_q(\mathbf{r}, 0) = \exp(-i\frac{\pi q y^2}{\lambda f})\mathcal{L}_p^l(\mathbf{r}/w_0)$. The form of $u_q(\mathbf{r}, 0)$ is comparable with Eq. (8) by setting $c_x = 0$ and $c_y = -qz_R/f$. By employing Eq. (3), the complex amplitude of the light field can be expressed as

$$\Psi(\mathbf{r}, z) = e^{i\gamma x^2} \sum_{q=-\infty}^{+\infty} t_q e^{-i\gamma x_q^2} u_q(x_q, y, z), \tag{28}$$

where $x_q = x - \frac{q\lambda z}{\Lambda}$, and using Eq. (10),

$$u_q(x_q, y, z) \propto \frac{e^{i[\Phi_q(\mathbf{r})+\Theta_q]}}{\sqrt{|\sigma_x\sigma_{y,q}|}} \begin{cases} \mathcal{G}_{p+|l|,p}\left[\mathrm{R}\left(-\frac{\pi}{4}\right)\mathbf{r}_q|\frac{\pi}{4} - \omega_{-q}\right], & l \geq 0; \\ \mathcal{G}_{p,p+|l|}\left[\mathrm{R}\left(-\frac{\pi}{4}\right)\mathbf{r}_q|\frac{\pi}{4} - \omega_{-q}\right], & l < 0. \end{cases} \tag{29}$$

Here

$$\sigma_x = 1 + i\zeta, \quad \sigma_{y,q} = 1 - qz/f + i\zeta, \tag{30a}$$

$$\mathbf{r}_q = \left(\frac{x_q}{w_0|\sigma_x|}, \frac{y}{w_0|\sigma_{y,q}|}\right), \quad \omega_{\pm q} = \frac{\arg\sigma_{y,q} \pm \arg\sigma_x}{2}, \tag{30b}$$

$$\Phi_q(\mathbf{r}) = \frac{\zeta}{w_0^2|\sigma_x|^2}x_q^2 + \frac{c_y + (1 + c_y^2)\zeta}{w_0^2|\sigma_{y,q}|^2}y^2, \tag{30c}$$

$$\Theta_q = l(\pi/4) - (2p + |l| + 1)\omega_{+q}. \tag{30d}$$

An alternative approach based on Eq. (18) is presented in Supplement 1.

The propagation distance at which the LG-to-HG mode conversion is realized can be obtained by replacing f by f/q in Eq. (22) as follows:

$$\zeta_q = \frac{qz_R}{2f}\left[1 \pm \sqrt{1 - \left(\frac{2f}{qz_R}\right)^2}\right]. \tag{31}$$

Then the LG-to-HG mode conversion is realized for the diffraction orders with q provided that $2f \leq qz_R$ or equivalently $w_0 \geq \sqrt{2f\lambda/q\pi}$. If the LG-to-HG mode conversion requirement is fulfilled for the first diffraction order ($q = +1$), it will be fulfilled for the higher ones $q = +2, +3, \ldots$. For the case of $f \ll z_R$, the propagation distances can be estimated as follows:

$$z_{1,q}^{\mathrm{app}} \approx f/q, \quad z_{2,q}^{\mathrm{app}} \approx qz_R^2/f. \tag{32}$$

This result shows that LG-to-HG mode conversion occurs at different propagation distances for different diffraction orders, as shown in Fig. 7. The figure shows diffraction patterns from a quadratic curved-line grating at the conversion

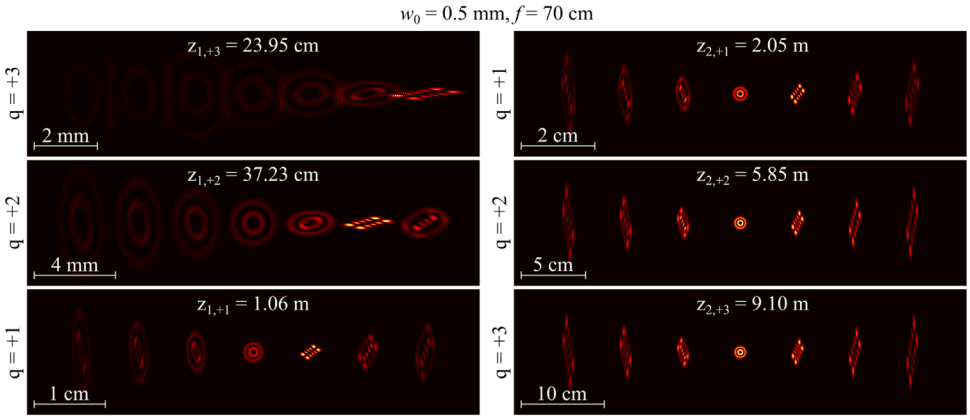

Fig. 7. Diffraction patterns of an LG beam having $\lambda = 532$ nm, $p = 1$, $l = 3$, and $w_0 = 0.5$ mm from a quadratic curved-line grating having $f = 70$ cm and $\Lambda = 0.07$ mm. The patterns are shown at the predicted distances for LG-to-HG mode conversion for various diffraction orders at the closer distance $z_{1,q}$ (left column) and far distance $z_{2,q}$ (right column). For additional details, see also Visualization 3.

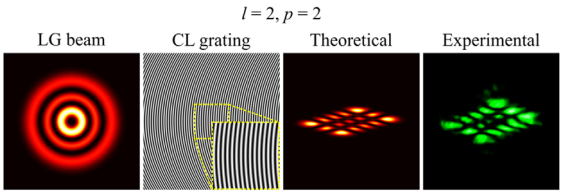

Fig. 8. Intensity pattern of an LG beam with $l = 2$ and $p = 2$ (beam waist $w_0 = 0.8$ mm), transmission through an amplitude quadratic curved-line grating (sinusoidal profile with $\Lambda = 0.1$ mm and $f = 94$ cm), and resulting theoretical (third column) and experimental (fourth column) diffracted patterns at $z = 80$ cm (see also Visualization 4).

distances for the first ($q = 1$), second ($q = 2$), and third ($q = 3$) orders. To enhance the visibility of the diffraction orders, the Fourier coefficients t_q were set equal for $q = 0, \pm 1$, and ± 2. Background Visualization 3 illustrates the dependence of LG-to-Hg mode conversion distance on diffraction orders in quadratic curved-line gratings.

Since in our previous work [27–29] we have studied this grating numerically and experimentally, we only study the theory and experiment here. In Fig. 8, we show the intensity pattern of an LG beam with $l = 2$ and $p = 2$ with $w_0 = 0.8$ mm, the transmission of a sinusoidal profile curved-line grating with amplitude quadratic with parameters $\Lambda = 0.1$ mm and $f = 94$ cm, and the resulting theoretical (third column) and experimental (fourth column) diffracted patterns at the propagation distance $z = 80$ cm, from left to right, respectively. Background Visualization 4 presents a calculated diffraction pattern of an LG beam as it passes through the quadratic curved-line grating, illustrating the LG-to-Hg mode conversion.

6. OFF-AXIS DIFFRACTION OF AN LG BEAM FROM ELLIPTICAL ZONE PLATE

The transmission function of an elliptical ZP, with the offset position of x_0 relative to the optical axis, can be expressed as a Fourier series:

$$t(\mathbf{r}) = \sum_{q=-\infty}^{+\infty} t_q \exp\left[\frac{-i\pi q}{\lambda}\left(\frac{(x-x_0)^2}{f_x} + \frac{y^2}{f_y}\right)\right]. \quad (33)$$

By considering the diffraction of an LG beam from an elliptical ZP, the complex amplitude immediately after the grating can be expressed as

$$\Psi(\mathbf{r}, +0) = \sum_{q=-\infty}^{+\infty} t_q \exp\left(i\frac{2\pi q x_0 x}{\lambda f_x}\right) u_q(\mathbf{r}, 0), \quad (34)$$

where

$$u_q(\mathbf{r}, 0) = \exp\left(\frac{-i\pi q x_0^2}{\lambda f_x}\right) \exp\left[\frac{-i\pi q}{\lambda}\left(\frac{x^2}{f_x} + \frac{y^2}{f_y}\right)\right] \mathcal{L}_p^l(\mathbf{r}/w_0). \quad (35)$$

Clearly, $u_q(\mathbf{r}, 0)$ is comparable with Eq. (8) by setting $c_x = -qz_R/f_x$ and $c_y = -qz_R/f_y$. The complex amplitude of the diffracted light field can be expressed as

$$\Psi(\mathbf{r}, z) = e^{i\gamma x^2} \sum_{q=-\infty}^{+\infty} t_q e^{-i\gamma x_q^2} u_q(x_q, y, z), \quad (36)$$

by using Eq. (3), where $x_q = x - \frac{qz}{f_x}x_0$, and employing Eq. (10):

$$u_q(x_q, y, z) \propto \frac{e^{i[\Phi_q(\mathbf{r})+\Theta_q]}}{\sqrt{|\sigma_{x,q}\sigma_{y,q}|}} \begin{cases} \mathcal{G}_{p+|l|,p}\left[\mathrm{R}\left(-\frac{\pi}{4}\right)\mathbf{r}_q | \frac{\pi}{4} - \omega_{-q}\right], & l \geq 0; \\ \mathcal{G}_{p,p+|l|}\left[\mathrm{R}\left(-\frac{\pi}{4}\right)\mathbf{r}_q | \frac{\pi}{4} - \omega_{-q}\right], & l < 0, \end{cases} \quad (37)$$

where

$$\sigma_{x,q} = 1 - qz/f_x + i\zeta, \quad \sigma_{y,q} = 1 - qz/f_y + i\zeta,$$

$$\mathbf{r}_q = \left(\frac{x_q}{w_0|\sigma_{x,q}|}, \frac{y}{w_0|\sigma_{y,q}|}\right), \quad (38a)$$

$$\Phi_q(\mathbf{r}) = \frac{c_x + (1+c_x^2)\zeta}{w_0^2|\sigma_{x,q}|^2} x_q^2 + \frac{c_y + (1+c_y^2)\zeta}{w_0^2|\sigma_{y,q}|^2} y^2,$$

$$\omega_{\pm q} = \frac{\arg\sigma_{y,q} \pm \arg\sigma_{x,q}}{2}, \quad (38b)$$

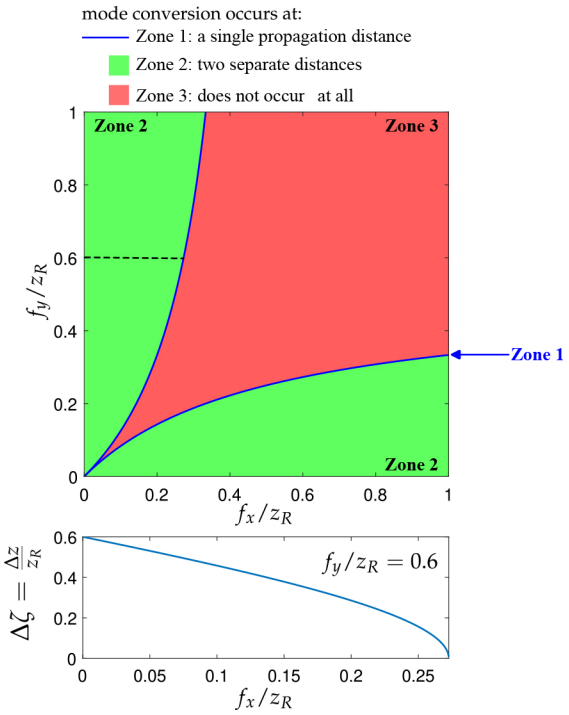

Fig. 9. Top: regions of f_x and f_y where LG-to-HG mode conversion occurs twice (Zone 2), once (Zone 1), or never (Zone 3). Bottom: spatial separation of LG-to-HG conversion planes for the first diffraction order and $f_y/z_R = 0.6$; the dashed line in the top row indicates the f_x/z_R range.

$$\Theta_q = l(\pi/4) - (2p + |l| + 1)\omega_{+q} - \frac{\pi q x_0^2}{\lambda f_x}. \tag{38c}$$

Here again an alternative approach based on Eq. (18) is presented in Supplement 1.

By considering $c_x = -qz_R/f_x$ and $c_y = -qz_R/f_y$, the condition $|c_x - c_y| \geq 2$ for the realization of the LG-to-HG mode conversion leads to

$$\left|\frac{z_R}{f_x} - \frac{z_R}{f_y}\right| \geq \frac{2}{q}. \tag{39}$$

This result shows that if the condition is fulfilled for the first diffraction order ($q = 1$), it will also be fulfilled for higher orders.

Figure 9 illustrates LG-to-HG mode conversion behavior in parameter space (f_x, f_y): the top panel shows regions of double (green), single (blue), and no conversion (red), and the bottom panel displays the separation of conversion planes for the first diffraction order and $f_y/z_R = 0.6$, with the range of f_x/z_R values shown by the dashed line in the top panel.

Figure 10 illustrates the three conversion scenarios (twice, once, and never) by showing the propagation of an LG beam from elliptical ZPs with varying f_x and f_y values.

It is worth noting that for sinusoidal gratings, the summations involve only three terms corresponding to $q = -1$, 0, and 1. In Fig. 11, we show the off-axis diffraction of an LG beam with $l = 2$, $p = 2$, and $w_0 = 0.8$ mm from pure-amplitude (a), (b) and pure-phase (c), (d) elliptical ZPs of sinusoidal profile. In (a) and (c), the parameters are $f_x = 70$ cm, $f_y = 3f_x$, and $x_0 = 5$ mm, and the propagation distance $z = \frac{1}{4}f_x + \frac{3}{4}f_y$. For (b) and (d), the parameters are swapped, with $f_y = 70$ cm, $f_x = 3f_y$, and $x_0 = 5$ mm, while the propagation distance becomes $z = \frac{1}{4}f_y + \frac{3}{4}f_x$.

We can infer from the figure that the swapping of f_x and f_y results in a reversal of the rotation direction of the diffracted pattern. It is also important to note that the sign of the TC of the incident beam affects the rotation direction as well. In Fig. 12, we exhibit the first-order diffraction patterns of intensity in the experiment (green) and theory (red). In all three cases, $f_x = 70$ cm, $f_y = 3F_x$, $\lambda = 532$ nm, and $l = 2$; $w_0 = 0.6$ mm

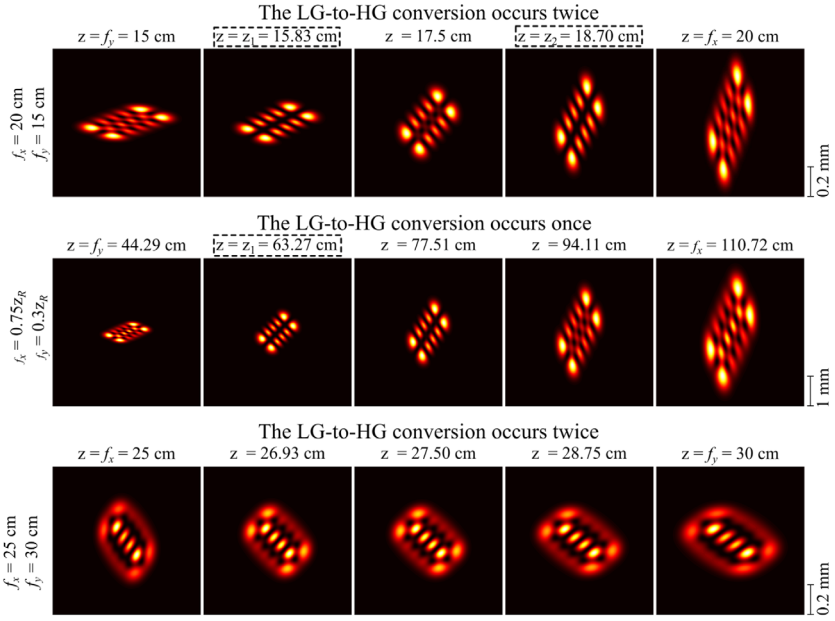

Fig. 10. Propagation of an LG beam with $\lambda = 532$ nm, $p = 1$, $l = 3$, and $w_0 = 0.5$ mm from elliptical ZPs having various values of f_x and f_y so that LG-to-HG mode conversion occurs twice (first row), once (second row), or never (third row).

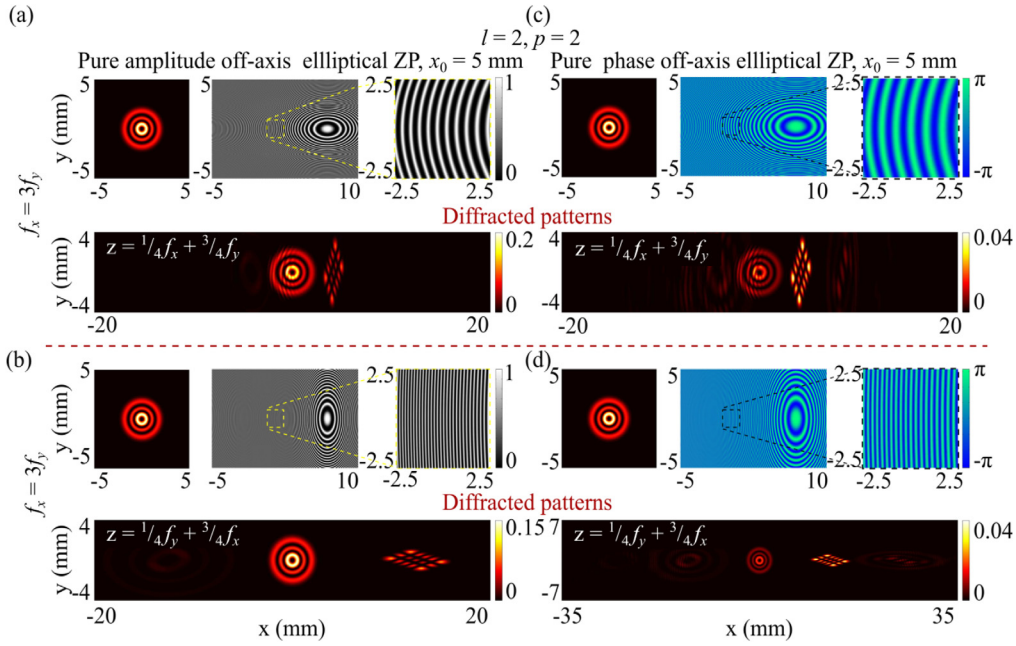

Fig. 11. Theoretical prediction for the characterization of an LG beam with parameters $l = 2$, $p = 2$, and beam waist $w_0 = 0.8$ mm, using either pure-amplitude (a), (b) or pure-phase (c), (d) elliptical ZPs with sinusoidal profiles under off-axis illumination. In (a) and (c), the parameters are $f_x = 70$ cm, $f_y = 3f_x$, and $x_0 = 5$ mm, and the propagation distance $z = \frac{1}{4}f_x + \frac{3}{4}f_y$, and for (b) and (d), the parameters are $f_y = 70$ cm, $f_x = 3f_y$, $x_0 = 5$ mm, and $z = \frac{1}{4}f_y + \frac{3}{4}f_x$. For additional details, see also Visualization 5, Visualization 6, and Visualization 7.

for $p = 0$, $w_0 = 0.7$ mm for $p = 1$, and $w_0 = 0.8$ mm for $p = 2$. As LG beams are transmitted through pure-phase elliptical ZPs with a sinusoidal profile under off-axis illumination, they produce a two-dimensional array of light spots. The TC and the radial index of the primary beam can be determined by enumerating these spots in both dimensions. For beams, the number of intensity spots along one axis is given by $p + 1$, while it is $p + l + 1$ along the other axis. If the radial index is zero, there are $l + 1$ spots located along the same line. Even in the absence of astigmatism-induced aberrations, the radial index can be determined by counting the intensity rings around the central ring in the transverse profile. However, astigmatism-induced aberrations must be introduced to determine the TC of a beam. This step facilitates the LG-to-HG mode conversion, which is essential for characterizing the input LG beam, as the spot count depends on both the radial index and the TC. The background Visualization 5 and Visualization 6 provide detailed theoretical diffraction patterns of an LG beam with $l = 2$ and $p = 2$ passing through pure-amplitude and pure-phase elliptical ZPs under off-axis illumination at various propagation distances. Additionally, background Visualization 7 illustrates the effect of off-axis illumination on a pure-amplitude elliptical ZP by showing the diffraction pattern of an LG beam at the propagation distance of $z = 175$ cm for different off-axis values in the x direction. The obtained diffraction patterns affirm that optical elements with astigmatic aberrations can be employed to reveal the presence of TC and radial index of a vortex beam.

7. SUMMARY

In summary, our study revisits and refines the existing theoretical framework of LG-to-HG mode conversion using astigmatism while also introducing a new independent approach based on expanding LG modes in terms of HG modes. Our central goal is to determine the conditions and propagation distances for this mode conversion. The framework is applied to analyze the diffraction of LG beams by cylindrical lenses, quadratic curved-line gratings, and elliptical ZPs. A key finding is that for quadratic curved-line gratings and elliptical ZPs, the LG-to-HG conversion and its distance are dependent on the diffraction order. We also investigated the far-field propagation of astigmatic LG beams using two independent methods, resulting in a useful formula potentially applicable beyond paraxial optics. Finally, the work explores two types of astigmatic phases that allow for controllable LG-to-HG conversion, specifically enabling the control over the stretching and orientation of the resulting HG modes. Our theoretical results are in excellent qualitative agreement with our experiments. Our work developed a theoretical model to describe the interaction of an optical vortex with astigmatic optical elements. It might also facilitate the design of new mode converter elements.

Funding. Institute for Advanced Studies in Basic Sciences (G2024IASBS12632); Center for International Scientific Studies and Collaboration (CISSC) of Iran (4020667); Natural Sciences and Engineering Research Council of Canada (RGPIN-2018-05497).

Acknowledgment. The author Davud Hebri would like to acknowledge the Izaak Walton Killam Postdoctoral fellowship.

Disclosures. The authors declare no conflicts of interest.

Data availability. No data were generated or analyzed in the presented research.

Supplemental document. See Supplement 1 for supporting information of the methodology used.

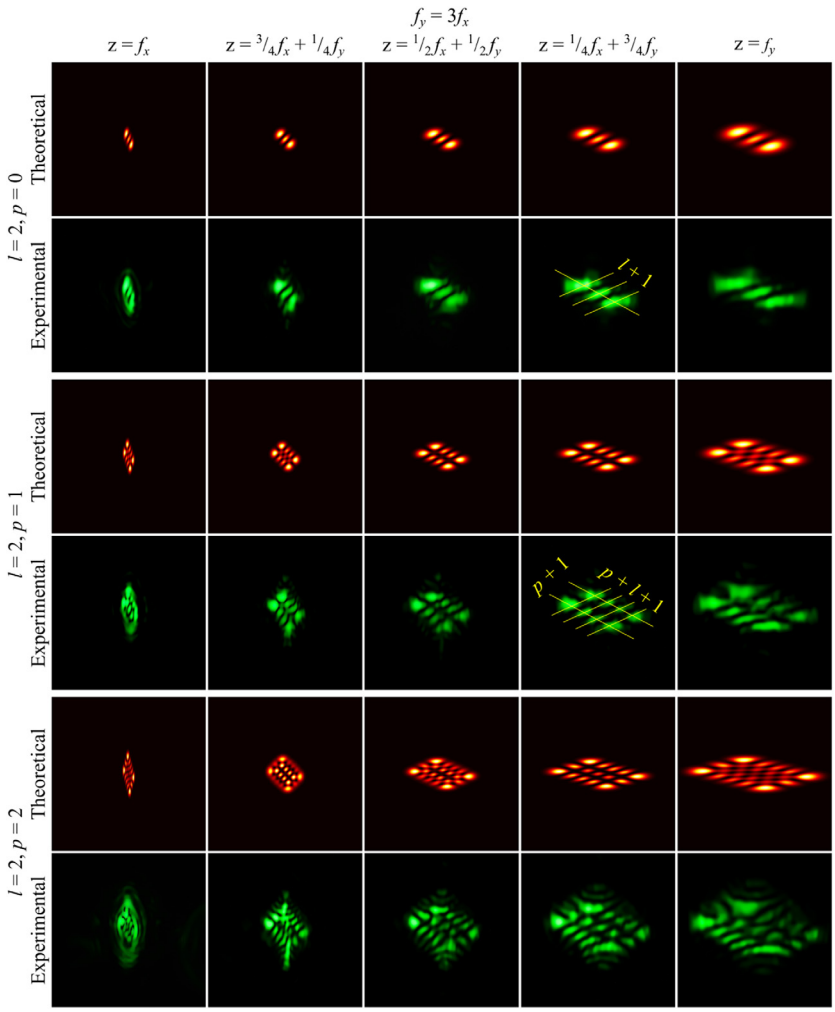

Fig. 12. First-order diffraction patterns of LG beam intensities for given l and p behind a ZP of the sinusoidal profile under off-axis illumination in experiment (green) and theory (red). Other parameters are $f_x = 70$ cm, $f_y = 3f_x$, $\lambda = 532$ nm, and $l = 2$; $w_0 = 0.6$ mm for $p = 0$, $w_0 = 0.7$ mm for $p = 1$, and $w_0 = 0.8$ mm for $p = 2$.

REFERENCES

1. M. Padgett, J. Courtial, and L. Allen, "Light's orbital angular momentum," Phys. Today **57**(5), 35–40 (2004).
2. L. Allen, S. M. Barnett, and M. J. Padgett, *Optical Angular Momentum* (CRC Press, 2003).
3. G. Gbur and R. K. Tyson, "Vortex beam propagation through atmospheric turbulence and topological charge conservation," J. Opt. Soc. Am. A **25**, 225–230 (2007).
4. A. M. Yao and M. J. Padgett, "Orbital angular momentum: origins, behavior and applications," Adv. Opt. Photonics **3**, 161–204 (2011).
5. G. J. Gbur, *Singular Optics* (CRC Press, 2017).
6. H. He, M. Friese, N. Heckenberg, *et al.*, "Direct observation of transfer of angular momentum to absorptive particles from a laser beam with a phase singularity," Phys. Rev. Lett. **75**, 826 (1995).
7. A. Terray, J. Oakey, and D. W. Marr, "Microfluidic control using colloidal devices," Science **296**, 1841–1844 (2002).
8. G. Gibson, J. Courtial, M. J. Padgett, *et al.*, "Free-space information transfer using light beams carrying orbital angular momentum," Opt. Express **12**, 5448–5456 (2004).
9. A. Mair, A. Vaziri, G. Weihs, *et al.*, "Entanglement of the orbital angular momentum states of photonics," Nature **412**, 313–316 (2001).
10. L. Allen, M. W. Beijersbergen, R. Spreeuw, *et al.*, "Orbital angular momentum of light and the transformation of Laguerre-Gaussian laser modes," Phys. Rev. A **45**, 8185 (1992).
11. M. Harris, C. Hill, P. Tapster, *et al.*, "Laser modes with helical wave fronts," Phys Rev. A **49**, 3119 (1994).
12. C.-S. Guo, L.-L. Lu, and H.-T. Wang, "Characterizing topological charge of optical vortices by using an annular aperture," Opt. Lett. **34**, 3686–3688 (2009).
13. J. Hickmann, E. Fonseca, W. Soares, *et al.*, "Unveiling a truncated optical lattice associated with a triangular aperture using light's orbital angular momentum," Phys. Rev. Lett. **105**, 053904 (2010).
14. L. E. de Araujo and M. E. Anderson, "Measuring vortex charge with a triangular aperture," Opt. Lett. **36**, 787–789 (2011).
15. D. Hebri, S. Rasouli, and A. M. Dezfouli, "Theory of diffraction of vortex beams from structured apertures and generation of elegant elliptical vortex Hermite–Gaussian beams," J. Opt. Soc. Am. A **36**, 839–852 (2019).
16. J. Zhou, W. Zhang, and L. Chen, "Experimental detection of high-order or fractional orbital angular momentum of light based on a robust mode converter," Appl. Phys. Lett. **108**, 111108 (2016).
17. A. Volyar, M. Bretsko, Y. Akimova, *et al.*, "Measurement of the vortex and orbital angular momentum spectra with a single cylindrical lens," Appl. Opt. **58**, 5748–5755 (2019).
18. V. V. Kotlyar, A. A. Kovalev, and A. P. Porfirev, "Astigmatic transforms of an optical vortex for measurement of its topological charge," Appl. Opt. **56**, 4095–4104 (2017).

19. X. Fang, Z. Kuang, P. Chen, *et al.*, "Examining second-harmonic generation of high-order Laguerre–Gaussian modes through a single cylindrical lens," Opt. Lett. **42**, 4387–4390 (2017).
20. P. Liu, Y. Cao, Z. Lu, *et al.*, "Probing arbitrary Laguerre–Gaussian beams and pairs through a tilted biconvex lens," J. Opt. **23**, 025002 (2021).
21. I. Moreno, J. A. Davis, B. M. L. Pascoguin, *et al.*, "Vortex sensing diffraction gratings," Opt. Lett. **34**, 2927–2929 (2009).
22. S. Zheng and J. Wang, "Measuring orbital angular momentum (OAM) states of vortex beams with annular gratings," Sci. Rep. **7**, 40781 (2017).
23. L. Janicijevic, S. Topuzoski, L. Stoyanov, *et al.*, "Diffraction of a Gaussian beam by a four-sector binary grating with a shift between adjacent sectors," Opt. Commun. **389**, 203–211 (2017).
24. K. Dai, C. Gao, L. Zhong, *et al.*, "Measuring OAM states of light beams with gradually-changing-period gratings," Opt. Lett. **40**, 562–565 (2015).
25. D. Hebri, S. Rasouli, and M. Yeganeh, "Intensity-based measuring of the topological charge alteration by the diffraction of vortex beams from amplitude sinusoidal radial gratings," J. Opt. Soc. Am. B **35**, 724–730 (2018).
26. P. Panthong, S. Srisuphaphon, A. Pattanaporkratana, *et al.*, "A study of optical vortices with the Talbot effect," J. Opt. **18**, 035602 (2016).
27. P. Amiri, A. M. Dezfouli, and S. Rasouli, "Efficient characterization of optical vortices via diffraction from parabolic-line linear gratings," J. Opt. Soc. Am. B **37**, 2668–2677 (2020).
28. S. Rasouli, S. Fathollazade, and P. Amiri, "Simple, efficient and reliable characterization of Laguerre-Gaussian beams with non-zero radial indices in diffraction from an amplitude parabolic-line linear grating," Opt. Express **29**, 29661–29675 (2021).
29. S. Rasouli, P. Amiri, V. V. Kotlyar, *et al.*, "Characterization of a pair of superposed vortex beams having different winding numbers via diffraction from a quadratic curved-line grating," J. Opt. Soc. Am. B **38**, 2267–2276 (2021).
30. S. Rasouli, P. Amiri, and D. Hebri, "Transformation of Laguerre-Gaussian beams into 1D array of Hermite-Gaussian modes under the Talbot effect," Opt. Express **31**, 20683–20695 (2023).
31. E. Abramochkin and V. Volostnikov, "Beam transformations and nontransformed beams," Opt. Commun. **83**, 123–135 (1991).
32. E. Abramochkin and V. Volostnikov, "Generalized Gaussian beams," J. Opt. A **6**, S157 (2004).
33. E. Abramochkin, E. Razueva, and V. Volostnikov, "General astigmatic transform of Hermite–Laguerre–Gaussian beams," J. Opt. Soc. Am. A **27**, 2506–2513 (2010).
34. B. E. Saleh and M. C. Teich, *Fundamentals of Photonics* (Wiley, 2019).
35. A. E. Siegman, *Lasers* (University Science Books, 1986).
36. E. Abramochkin and V. Volostnikov, "Generalized Hermite-Laguerre-Gauss beams," Phys. Wave Phenom. **18**, 14–22 (2010).
37. A. Wada, T. Ohtani, Y. Miyamoto, *et al.*, "Propagation analysis of the Laguerre–Gaussian beam with astigmatism," J. Opt. Soc. Am. A **22**, 2746–2755 (2005).
38. S. A. Akhmanov and S. Y. Nikitin, *Physical Optics* (Oxford University, 1997).
39. P. Amiri, S. Rasouli, D. Hebri, *et al.*, "Talbot-effect-based multiplication of Laguerre–Gaussian beams with non-zero radial indices: from theory to experimental realization," Opt. Commun. **574**, 131203 (2025).